Optimized Characteristics of a Designed Oxide Confined 420nm MQW Blue-Violet Laser by Varying Differential Gain

Nadia Afroze
Department of EEE
American International University-Bangladesh
Dhaka, Bangladesh
afrozenadia60@gmail.com

Rinku Basak
Department of EEE
American International University-Bangladesh
Dhaka, Bangladesh
rinku_biju@yahoo.com

***Abstract*— In this work, the performance characteristics of a designed oxide confined 420nm InGaN based multiple quantum well (MQW) blue-violet laser have been optimized and presented by varying differential gain. The material gain of $In_{0.1227}Ga_{0.8773}N/Al_{0.08}Ga_{0.92}N$ MQW edge emitting laser (EEL) has been theoretically obtained. The peak material gain obtained from the analysis has been used to study the performance of the designed oxide confined laser. The lower value of the threshold current has been obtained as 3.4mA for the designed oxide confined laser. The steady state output power is 71.68mW and the modulation bandwidth is 14GHz at a differential gain of $1x10^{-16}$ cm^2. By increasing the differential gain up to $5x10^{-16}$ cm^2 a maximum value of output power is obtained as 73.37mW and a maximum modulation bandwidth is obtained as 28GHz. Thus, a better performance of the designed oxide confined laser has been observed by varying the differential gain.**

Keywords—blue-violet laser; oxide confined; modulation bandwidth; differential gain.

I. INTRODUCTION

Semiconductor laser diodes with blue beams are typically based on gallium (III) nitride (GaN, violet color) or indium gallium nitride (often true blue in color, but also able to produce other colors). Both blue and violet lasers can also be constructed using frequency-doubling of infrared laser wavelengths from diode lasers or diode-pumped lasers. The laser diode can be designed for different emission wavelengths based on applications. Semiconductor laser diodes are also at the heart of Laser TV, Laser printers, barcode scanners, laser printers and security devices etc. The best semiconductor for blue-violet lasers is gallium nitride (GaN) crystals, which are much harder to manufacture, requiring higher pressures and temperatures. The active layer of the Nichia devices was formed from InGaN quantum wells. The new invention enabled the development of small, convenient and low-priced blue-violet, ultraviolet UV lasers and opened the way for applications such as high-density HD DVD data storage and Blue-ray discs. The shorter wavelength allows it to read discs containing much more information [1]. If shorter wavelengths such as blue and U.V. are used, more information can be collected on optical storage devices. Normal DVD formats use 680nm but the more popular blue-ray discs work at 405nm. The blue-ray discs hold 50 gigabyte of information which is 5-10 times more than DVDs. Research is going on already to develop the next generation of laser diodes that will work in the deep U.V. range.

In this work, the performance characteristics of a 420nm designed oxide confined laser is presented with the aim of obtaining high performance characteristics for the designed oxide confined laser by varying differential gain.

II. LASER MODEL

In this work, an EEL whose active region contains three QWs of $In_{0.1227}Ga_{0.8773}N$, separated by $Al_{0.08}Ga_{0.92}N$ barriers are chosen for simulation with a view to obtain 420nm operation. The cavity of the EEL consisting of two cladding layers of $Al_{0.16}Ga_{0.84}N$. The cladding and active layer materials are separated by two separate confinement heterostructure (SCH) layers of $Al_{0.08}Ga_{0.92}N$.

For achieving high performance, the In, Ga and N concentrations of the InGaN QW material is chosen by computing the concentration values using Vegard's law [2]. Values of a required number of parameters are obtained from different published sources [3].

The band gap energy of InGaN is given by-

$$E_g(In_xGa_{1-x}N)\ [eV] = E_g(InN)x + E_g(GaN)(1-x) - bx(1-x) \quad (1)$$

where b is the bowing parameter.

The structure of a blue-violet laser, presented in Fig. 1, consists of active region, barriers, cladding and oxide confinement layers. The active region of a blue-violet laser contains 3 QWs of $In_{0.1227}Ga_{0.8773}N$ (band gap energy, E_{gw}=2.8232eV; refractive index, n=2.6183) of 5nm each and 2 barriers of $Al_{0.08}Ga_{0.92}N$ (band gap energy, E_{gb}=3.5767eV; refractive index, n=2.4723) of 7nm each. The reason for selecting fractional compositions for QW material $In_{0.1227}Ga_{0.8773}N$ up to 4 decimal places is to calculate the band

gap energy more accurately for the lasing to occur exactly at 420.3nm.

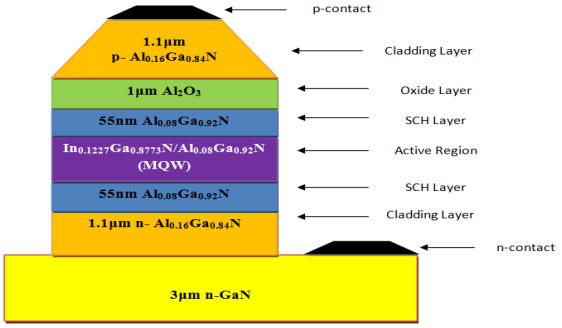

Fig. 1. The designed structure of a 420nm $In_{0.1227}Ga_{0.8773}N$/ $Al_{0.08}Ga_{0.92}N$ MQW Oxide Confined Blue-Violet Laser.

The electron effective mass (m_e) is $0.18443m_o$ and the hole effective mass (m_h) is $0.29356m_o$ of the QW material, where m_o is the mass of electron. The total thickness of the active region is 29nm considering 3 QWs and 2 barriers; the width is 2µm (without oxide confinement layer) and the length is 780µm.

The active region of the laser is sandwiched between two separate confinement heterostructure (SCH) layers of $Al_{0.08}Ga_{0.92}N$ (E_{gb}=3.5767eV, n=2.4723) of 55nm each. The total thickness of the cavity including SCH is calculated as 139nm. After adding the 1µm oxide confinement layer of Al_2O_3, the new width of the active region is 0.67µm. The p-type and n-type cladding layers of $Al_{0.16}Ga_{0.84}N$ (E_{gclad}=3.7458eV, n=2.4379) are of 1.1µm each. The confinement factor is calculated as Γ=0.2086. The n-GaN substrate of 3µm is connected with the lower n-contact and the upper p-contact is connected with the p-cladding layer as shown in Fig. 1.

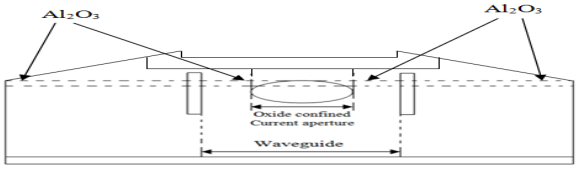

Fig. 2. Cross Sectional View of a 420nm $In_{0.1227}Ga_{0.8773}N$/ $Al_{0.08}Ga_{0.92}N$ MQW Oxide Confined Blue-Violet Laser.

Fig. 2 shows the cross-sectional view of the designed oxide-confined layer. The procedure of oxide confinement considered in this work is based on other research work [4]. The lattice and thermal mismatch occurs if something is grown on top of oxide layer. The insulating silica layer is used on the top of the central waveguide in fabrication process [4]. The silicon on insulator (SOI) is used to reduce the lattice and thermal mismatch [5]. To use the oxide confinement layer, the width has been reduced from 2µm to 0.67µm. As a result the active volume of the active region reduces from $4.524x10^{-11}$ cm^3 to $1.51554x10^{-11}$ cm^3 and the threshold current reduces from 10mA to 3.4mA.

III. Simulations Results And Discussions

A. Computation of Transparency Carrier Density N_{tr}, Threshold Carrier Density N_{th}, Photon Life Time τ_p and Threshold Current I_{th} of the Designed Laser

The transparency carrier density of a material is related to the effective masses of carriers in the conduction band (CB) and valance band (VB) as [2], [6-8]

$$N_{tr} = 2\left(\frac{kT}{2\pi\hbar^2}\right)^{\frac{3}{2}}(m_c m_v)^{\frac{3}{4}} \quad (2)$$

where k is the Boltzmann constant, T is the temperature in K, $\hbar$ is the Plank's constant divided by 2π, m_c and m_v are the effective masses of the carrier in the CB and VB, respectively. The relationship is used to compute the transparency carrier density of the QW material. At 300K, the calculated value of transparency carrier density for $In_{0.1227}Ga_{0.8773}N$ is $2.8x10^{18}$ cm^{-3}. This value is lower than that of the barrier material for which it is suitable to be used as the QW material.

At 300K, the threshold carrier density of the $3.0079x10^{18}$ cm^{-3} has been found using the following expression [2]

$$N_{th} = N_{tr}e^{\frac{<\alpha_i>+\alpha_m}{\Gamma g_o}} \quad (3)$$

where g_o is the material gain constant.

Using the obtained threshold carrier density, the photon lifetime is then calculated using the following expression [2]

$$\tau_p = \frac{1}{v_g(<\alpha_i>+\alpha_m)} \quad (4)$$

The photon life, from the above expression is 4.3269ps with a group velocity v_g of $1.1786x10^{10}$cms^{-1}. The threshold current is then calculated using [2]

$$I_{th} = \frac{qV_a N_{th}}{\eta_i \tau_a} \quad (5)$$

It is found that at 300K the threshold current is as small as 3.4mA with an injection current efficiency (η_i) of 0.8.

B. Calculation of material gain

For designing an EEL structure the material gain is calculated as [2], [6-8]

$$g(E) = \left(\frac{q^2\pi\hbar}{\varepsilon_o m_o^2 ncE}\right)|M_T|^2\rho_r(f_2 - f_1) \quad (6)$$

where, q is the electron charge, ε_o is the free-space permittivity, c is the speed of light in vacuum, E is the transition energy, n is the refractive index of the laser structure, $|M_T|^2$ is the transition momentum matrix element, ρ_r is the reduced density of state, $\hbar$ is the Planck's constant divided by 2π, f_2 and f_1 are the electron quasi-Fermi functions in the conduction and valence band respectively.

Using Eq. (6), a peak material gain value of 1101cm^{-1} is obtained for $In_{0.1227}Ga_{0.8773}N/Al_{0.08}Ga_{0.92}N$ MQW EEL around the lasing wavelength of 428.1nm.

C. Calculation of Carrier Density, Photon Density and Output Power

The rate equations of a semiconductor laser are [2]

$$\frac{dN}{dt} = \frac{\eta_i I}{qV_a} - \frac{N}{\tau_c} - \frac{v_g a(N-N_{tr})S}{1+\varepsilon S} \tag{7}$$

and,

$$\frac{dS}{dt} = \frac{\Gamma v_g a(N-N_{tr})S}{1+\varepsilon S} + \Gamma\beta_{sp}\frac{\eta_i I_{th}}{q} - \frac{S}{\tau_p} \tag{8}$$

A plot of carrier density versus time is shown in Fig. 3 of the designed oxide confined laser for the different values of differential gain.

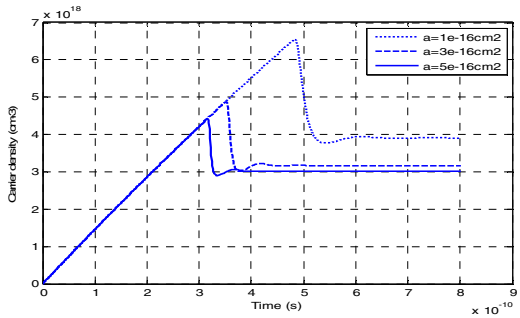

Fig. 3. Plots of Carrier Density versus Time of the designed oxide confined 420nm Laser for different values of differential gain.

The solution of these rate equations have been obtained using the parameter values and the finite difference method in MATLAB for the chosen value of injection current of 45mA, for the designed oxide confined 420nm laser.

The value of injection current should be such that it is above the threshold current. The plots of Fig. 3 show that the steady state carrier density is $3.909\text{x}10^{18}$ cm^{-3} for the designed oxide confined laser at a differential gain of $1\text{x}10^{-16}$ cm^2. As the differential gain is increased, the steady state carrier density decreases. The steady state carrier density is obtained as $3.023\text{x}10^{18}$ cm^{-3} at a differential gain of $5\text{x}10^{-16}$ cm^2. When the differential gain reaches $5.4\ \text{x}10^{-16}$ cm^2, the steady state carrier density is obtained as $3.004\text{x}10^{18}$ cm^{-3}, which is less than the threshold carrier density.

Using Eq. (8), the maximum steady state photon density is obtained as $1.231\text{x}10^{16}$ cm^{-3} at a differential gain of $5\text{x}10^{-16}$ cm^2.

With the aid of the varying nature of the photon density simulation, variation of output power can also be obtained from [2]

$$P_{out} = v_g \alpha_m h\nu S V_p \tag{9}$$

The output power of the designed laser can also be expressed in terms of material gain g, mirror loss coefficient α_m, injection current I and threshold current I_{th} as [2]

$$P_{out} = \frac{\alpha_m h\nu \eta_i}{qg\Gamma}(I - I_{th}) \tag{10}$$

Using, the output power of Eq. (9) and the parameter values presented above, plots of output power versus time of the designed oxide confined laser for the different values of differential gain are presented in Fig. 4 after computations.

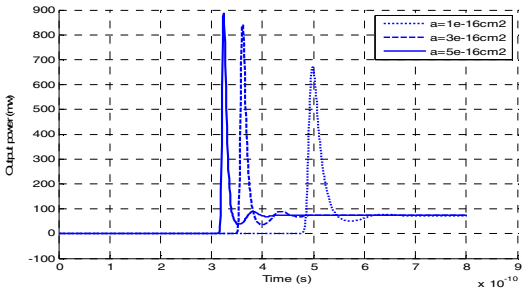

Fig. 4. Plots of Output power versus Time of the designed oxide confined 420nm Laser for different values of differential gain.

The plots of output power vs. time (in Fig. 4) show that the steady state output power is 71.68mW for the designed oxide confined laser at a differential gain of $1\text{x}10^{-16}$ cm^2. The steady state output power increases with the increasing value of differential gain. The maximum steady state output power has been obtained as 73.37mW at a differential gain of $5\text{x}10^{-16}$ cm^2.

The plot of output power versus wavelength is shown in Fig. 5 for the designed oxide confined laser at an injection current 45mA.

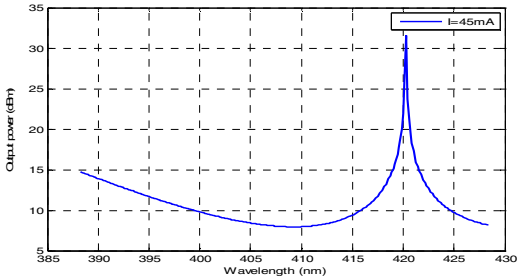

Fig. 5. Plot of Output Power versus Wavelength of the Designed Oxide Confined Laser at 300K, where injection current is 45mA. A Peak Intensity of the Power is obtained at 420.3nm Wavelength.

From Fig. 5 it is observed that the output power has its peak value 31.5dBm at 420.3nm, which is the wavelength of the designed oxide confined laser.

D. Modulation Response of the Designed Laser

The modulation response of the designed laser has been obtained using the equation of the transfer function as given below [2], [6-8]

$$H(f) = \frac{f_R^2}{f_R^2 - f^2 + j\left(\frac{f}{2\pi}\gamma\right)} \tag{11}$$

where f_R is the resonance frequency and γ is the damping parameter of a laser.

The above equation has been used to plot the relative response versus frequency for the designed oxide confined

laser for the different values of differential gain as shown in Fig. 6.

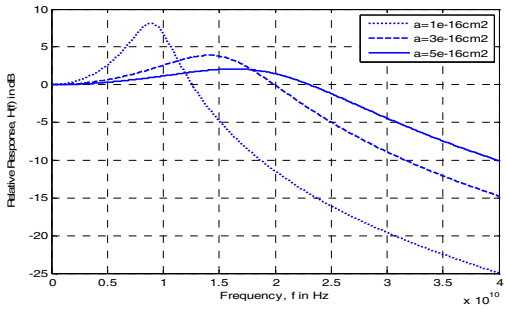

Fig. 6. Plots of Relative Response versus Frequency of the designed oxide confined 420nm Laser for different values of differential gain.

From Fig. 6 it has been found that the resonance frequency was 8.9GHz and modulation bandwidth was 14GHz for $1x10^{-16}$ cm^2 differential gain for the designed oxide confined laser. The resonance frequency and modulation bandwidth increases with the increasing value of differential gain. The maximum resonance frequency and modulation bandwidth has been obtained as 16.4GHz and 28GHz respectively at a differential gain of $5x10^{-16}$ cm^2.

IV. Conclusion

The performance characteristics of the designed oxide confined laser have been obtained by varying differential gain. The threshold current is found as 3.4mA for the designed oxide confined laser. If the differential gain is increased, all the observed characteristics such as the steady state carrier density have been found to decrease accordingly. When the value of differential gain reaches $5.4x10^{-16}$ cm^2, the threshold carrier density value exceeds the steady state value. As a result, the laser cannot operate anymore. If the differential gain is increased from $1x10^{-16}$ cm^2 to $5x10^{-16}$ cm^2, the maximum steady state output power increases from 71.68mW to 73.37mW, the modulation bandwidth increases from 14GHz to 28GHz and the resonance frequency increases from 8.9GHz to 16.4GHz. Therefore, a better performance is obtained with the increased differential gain which optimizes the laser design as desired.

References

[1] Arpad A. Bergh, "Blue Laser Diode (LD) and Light Emitting Diode (LED) Applications", Physica Status Solidi (a), Vol. 201, No. 12, pp. 2740–2754, September 10, 2004.

[2] L.A. Coldren, S.W. Corzine, Diode Lasers and Photonic Integrated Circuits, John Wiley, New York, pp. 1-263, 1995.

[3] Joachim Piprek, R. Kehl Sink, Monica A. Hansen, John E. Bowers, and Steve P. DenBaars, "Simulation and Optimization of 420nm InGaN/GaN Laser Diodes", Physics and Simulation of Optoelectronic Devices VIII, SPIE Proc. 3944, pp.1-12, 2000.

[4] Grant Erwin, A.C. Bryce, Richard M. De La Rue, "Low threshold oxide-confinement compact edge-emitting semiconductor laser diodes with high reflectivity 1D photonic crystal mirrors", Lasers and Applications, Proc. of SPIE Vol. 5958, October 11, 59580E-1-7p, 2005.

[5] Alexander A. Demkov, Agham B. Posadas, Intregration of Functional Oxides with Semiconductors, Springer, pp. 25-44, 2014.

[6] Rinku Basak, "Optimized High Performance Characteristics of a Designed 420nm InGAN/AlGaN MQW Blue Violet Laser", American Academic & Scholarly Research Journal, Vol.5, No.4, pp.23-33, May 2013.

[7] Tawsif Ibne Alam, Md. Abdur Rahim, Rinku Basak, "Design and Performance Analysis of a 635nm $Ga_{0.5}In_{0.5}P$/ $(Al_{0.7}Ga_{0.3})_{0.5}In_{0.5}P$ Multiple Quantum Well Separate Confinement Heterostructure Red Laser Considering Thermal Limitation", Trends in Opto-Electro & Optical Communications, STM Journals, Vol.3, Issue 1, pp.11-17, 2013.

[8] Tamal Roy, Avijit Das, Sujon Howlader, Md. Ronok Hasan Rubel, and Rinku Basak, "Design and Performance Analysis of a 1550nm $Al_{0.09}Ga_{0.38}In_{0.53}As$/InP MQW VCSEL by Varying Injection Current", International Journal of Multidisciplinary Sciences and Engineering, Vol. 4, No. 2, pp. 10-15, February 2013.